Substitution Kinetics of $[Fe(PDT/PPDT)_n(phen)_m]^{2+}$ ($n \neq m$; $n,m = 1,2$) with 2,2′-Bipyridine, 1,10-Phenanthroline, and 2,2′,6,2″-Terpyridine

RAJESH BELLAM, DEOGRATIUS JAGANYI

School of Chemistry and Physics, University of KwaZulu-Natal, Private Bag X01, Scottsville, Pietermaritzburg, 3209, South Africa

Received 13 October 2016; revised 21 November 2016; accepted 21 November 2016

DOI 10.1002/kin.21066
Published online 23 January 2017 in Wiley Online Library (wileyonlinelibrary.com).

ABSTRACT: The triazines 3-(2-pyridyl)-5,6-diphenyl-1,2,4-triazine (PDT), 3-(4-phenyl-2-pyridyl)-5,6-diphenyl-1,2,4-triazine (PPDT), and 1,10-phenanthroline (phen) were coordinated to the Fe^{2+} ion to form $Fe(PDT)_2(phen)^{2+}$ **(1)**, $Fe(PPDT)_2(phen)^{2+}$ **(2)**, $Fe(PDT)(phen)_2^{2+}$, **(3)** and $Fe(PPDT)(phen)_2^{2+}$ **(4)**. The complexes were synthesized and characterized by mass spectroscopy and elemental analysis. The rate of substitution of these complexes by 2,2′-bipyridine (bpy), 1,10-phenanthroline (phen), and 2,2′,6,2″-terpyridine (terpy) was studied in a sodium acetate–acetic acid buffers over the range 3.6–5.6 at 25, 35, and 45°C under pseudo–first-order conditions. The reactions are first order with respect to the concentration of the complexes. The reaction rates increase with increasing [bpy/phen/terpy] and pH, whereas ionic strength has no influence on the rate of reaction. Plots of k_{obs} versus [bpy/phen/terpy] and $1/[H^+]$ are linear with positive slopes and significant y-intercepts. This indicates that the reactions proceed by both dissociative as well as associative pathways for which the associative pathway predominates the substitution kinetics. Observed temperature-depended rate constants at the three temperatures at which substitution reactions were studied together with the protonation constants of the substituting ligands (phen, bpy, terpy) were used to evaluate the specific rate constants (k_1 and k_2) and thermodynamic parameters (E_a, $\Delta H^{\#}$, $\Delta S^{\#}$, and $\Delta G^{\#}$). The reactivity order of the four complexes depends on the phenyl groups present on the triazine (PDT/PPDT)

Correspondence to: R. Bellam; e-mail: rajeshchowdarybellam@gmail.com.

Supporting Information is available in the online issue at www.wileyonlinelibrary.com.

molecule. The π-electrons on phenyl rings stabilizes the charge on the metal center by inductive donation of electrons toward the metal center resulting in a decrease in reactivity of the complex, and the order is **1** < **2** < **3** < **4**. The rate of substitution is also influenced by the basicity of the incoming ligand (bpy/phen/terpy), and it decreased in the order: phen > terpy > bpy. Higher rate constants, low E_a values, and more negative entropy of activation ($-\Delta S^{\#}$) values were observed for the associative path, revealing that substitution reactions at the octahedral iron(II) complexes by bpy, phen, and terpy occur predominantly by the associative mechanism. Density functional theory calculations support the interpretations. © 2017 Wiley Periodicals, Inc. Int J Chem Kinet 49: 182–196, 2017

INTRODUCTION

The chemistry of the polypyridyls such as 2,2′-bipyridine (bpy) [1], 1,10-phenanthroline (phen) [2], 2,2′,6,2″-terpyridine (terpy) [3], and 2,4,6-tri-pyridyl-1,3,5-s-triazine (TPTZ) [4] has been studied extensively. The common feature for these polypyridyls is the presence of α,α-diimine moiety, which facilitates the formation of high-intensity (high molar absorptivity) complexes with divalent metal ions such as Fe, Cu, and Ru through the formation of five-membered chelate rings with the metal center. Triazines are analogues of benzene ring where the three carbons are replaced with nitrogens. The isomer, 1,2,4-triazine, is the most reported isomer than the other two (1,2,3-triazine and 1,3,5-triazine) [5–7]. 1,2,4-Triazine and substituted triazines show antifungal [8], antiviral [9], anticancer [10], antibiotics [11], antiparasitic [12], anti-HIV [13], antianxiety, and antiinflammatory [14] activities, and its biochemical reactivity has been studied [15]. Phenyl-substituted 1,2,4-triazines such as 3-(2-pyridyl)-5,6-diphenyl)-1,2,4-triazine (PDT) and 3-(4-phenyl-2-pyridyl)-5,6-diphenyl)-1,2,4-triazine (PPDT) (Scheme 1) are an important subgroup of 1,2,4-triazines. We have taken up the complexes of these molecules to study their substitution behavior with nucleophiles such as bpy, phen, and terpy. These ligands are also give very intense colored iron(II) complexes, $Fe(PDT)_3^{2+}$(λ_{max} = 555 nm, $\varepsilon_{max} = 2.35 \times 10^4$ mol^{-1} dm^3 cm^{-1}) [16] and $Fe(PPDT)_3^{2+}$(λ_{max} = 564 nm, $\varepsilon_{max} = 2.87 \times 10^4$ mol^{-1} dm^3 cm^{-1}) [17] with iron(II). Schilt [18] has prepared and characterized mixed ligand complexes of iron(II)/iron(III)-cyanide-aromatic diimine. He has also in collaboration with Taylor [19] prepared mixed ligand complexes of the type $[Fe(phen)_nL_{3-n}]X_2$ and $[Fe(terpy)(TPTZ)]X_2$ (where n = 1 or 2, L = methyl, phenyl, nitro, or chloro-substituted phen, and X = perchlorate or iodide ion). Burgess and Haines [20] have reported mechanistic aspects of the formation of iron(II)-cyanide-phen and related systems. There are also reports of mixed ligand complexes of the type $[FeL_{2\times2}]^{2+}$ and $[FeLX_4]^{2+}$ (where L = phen or bpy and X = cyanide or oxalate ion [21–24] and $[FeLL'_2]^{2+}$) and $[FeL_2L']^{2+}$ (where L = phen, L′ = phen-5,6-dione and 4,7-dimethyl phen) [25,26]. In these studies, the focus was on the synthesis of mixed ligand complexes of Fe(II) and their characterization by mass spectroscopy, NMR, UV–visible, and IR studies. Most mixed ligand complexes of iron(II) have been used to investigate DNA-binding studies [26–28]. However, there are no reports on the substitution kinetics of the mixed ligand complexes of Fe(II). We have synthesized and characterized the mixed ligand complexes of iron(II) containing phen and triazine (PDT/PPDT) molecules, $Fe(PDT)_2(phen)^{2+}$(**1**), $Fe(PPDT)_2(phen)^{2+}$(**2**$Fe(PDT)(phen)_2^{2+}$), (**3**), and $Fe(PDT)(phen)_2^{2+}$ (**4**). This paper reports on the kinetic and mechanism of substitution reactions of complexes **1**–**4** by bpy, phen, and terpy in an acetate buffer in the pH range 3.6–5.6. The aim of this work is to provide an understanding of the trend in the reactivity of the chosen complexes in respect to the influence of the phenyl rings bound to the coordinated triazine ring. The nucleophilicity of incoming ligand toward the complexes was also investigated. The kinetic results are supported by theoretical calculations (density functional theory, DFT).

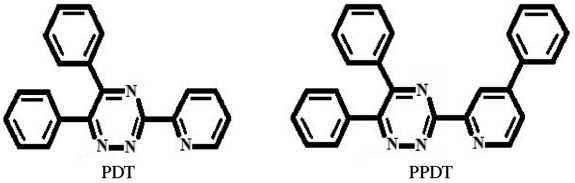

Scheme 1 Structures of triazine (PDT and PPDT) molecules.

EXPERIMENTAL

Reagents and Apparatus

Bpy, phen, terpy, iron(II) sulfate heptahydrate and sodium iodide (Sigma Aldrich) and PDT and PPDT

Table I Mass and Elemental Analysis Data of Complexes **1–4**

Complex/Molecular Formula		Yield	ESI-MS: *m/z* (%)	Elemental analysis	
				Calc.	Found
1	$[Fe(PDT)_2(phen)]I_2{\cdot}0.5H_2O$ ($C_{53}H_{40}FeI_2N_{10}{\cdot}0.5H_2O$)	448 mg (83%)	428.12 (M^{2+} –I_2, 100%)	C, 55.79; H, 3.33; N, 12.51; O, 0.71; Fe, 4.99	C, 55.57; H, 3.52; N, 12.62; O, 0.79; Fe, 4.97
2	$[Fe(PPDT)_2(phen)]I_2{\cdot}0.5H_2O$ ($C_{64}H_{44}FeI_2N_{10}{\cdot}0.5H_2O$)	530 mg (86%)	504.16 (M^{2+} –I, 74%)	C, 60.44; H, 3.57; N, 11.01; O, 0.63; Fe, 4.39	C, 60.49; H, 3.59; N, 11.03; O, 0.61; Fe, 4.36
3	$[Fe(PDT)(phen)_2]I_2{\cdot}2H_2O$ ($C_{44}H_{30}FeI_2N_8{\cdot}2H_2O$)	367 mg (77%)	428.11(M^{2+} –I, 86%), 363.08 (M^{2+} –I_2, 24%)	C, 51.99; H, 3.43; N, 11.12; O, 3.03; Fe, 5.49	C, 52.00; H, 3.37; N, 11.02; O, 3.09; Fe, 5.46
4	$[Fe(PPDT)(phen)_2]I_2{\cdot}H_2O$ ($C_{50}H_{34}FeI_2N_8{\cdot}H_2O$)	405 mg (79%)	401.12 (M^{2+} –I_2, 30%)	C, 55.89; H, 3.38; N, 10.43; O, 1.49; Fe, 5.20	C, 56.02; H, 3.44; N, 10.45; O, 1.53; Fe, 5.17

(GFS Chemicals Inc, Columbus, Ohio, USA) were used without further purification. Solutions of bpy, phen (0.01 mol dm^{-3} in 0.01 mol dm^{-3} HNO_3), and terpy (0.01 mol dm^{-3} in methanol) were prepared by dissolving requisite quantities. Acetate buffers of pH between 3.6 and 5.6 were prepared by mixing stoichiometric amounts of acetic acid (1.0 mol dm^{-3}) and sodium acetate (1.0 mol dm^{-3}). All these reagents were stored in amber-colored bottles. Electron-spray ionization (ESI) mass spectra of the complexes were recorded on a Waters TOF Micro-mass LCT Premier spectrometer operated in positive ion mode. Elementary compositions of the complexes were determined on a Thermoscientific CHNS-O analyzer Flash 2000. Iron(II) concentration was determined spectrophotometrically using 3-(2-pyridyl)-5,6-bis(4-sulfophenyl)-1,2,4-triazine (PDTS). Iron(II) forms a 1:3 complex with PDTS, $Fe(PDTS)_3^{4-}$ (λ_{max} = 562 nm and ε_{max} = 2.79×10^4 mol^{-1} dm^3 cm^{-1}) [29]. A 0.05-g sample of the complex was treated with 10 mL of 50% HNO_3. The solution was heated until all the organic matter was destroyed. The solution was then diluted to 100 mL. This solution was used for the estimation of iron(II) concentration. UV–visible spectra and kinetic measurements of slow reactions were recorded on a Varian Cary 100 Bio UV–visible spectrophotometer with a cell compartment thermostated by a Varian Peltier temperature controller accuracy of ±0.05°C.

Preparation of Mixed Ligand Complexes

The mixed ligand complexes reported in this paper were prepared according to the procedure of Taylor and Schilt [19]. Requisite quantities of PDT/PPDT (1.0 mmol) and phen (0.50 mmol) or PDT/PPDT (0.5 mmol) phen (1.0 mmol) were dissolved in 20 mL of hot ethyl alcohol. A solution of iron(II) sulfate heptahydrate (0.139 g, 0.50 mmol) in 5 mL of ultrapure water was added slowly dropwise with continuous stirring. The resultant solution was evaporated to 20 mL and filtered by a Millipore suction pump. Filtrate was cooled to room temperature, and a slight excess of sodium iodide (0.3 g) dissolved in 2 mL of water added dropwise. The resultant solution was cooled to –5°C for about 2 h, and the precipitate formed was separated by suction and washed several times with 5 mL aliquots of ice water then with diethyl ether and dried under vacuum. The mass and elemental analysis data are given in Table I, and the mass spectra for complexes are given in supplementary data S1 in the Supporting Information. The structures of the complexes **1–4** are shown in Scheme 2.

Kinetic Procedure

Kinetic runs were performed spectrophotometrically by monitoring the absorbance changes at λ_{max} values of the substrates as a function of time using a Cary 100 Bio UV–visible spectrophotometer. The spectral changes were recorded over the wavelengths range 350–700 nm. All kinetic runs were performed under pseudo–first-order conditions with [bpy/phen/terpy] over the [complex] in at least 10/20 fold excess. The absorbance changes were followed up to 10 half-lives. The effect of [complex] on the reaction was studied by carrying out kinetic runs at different concentrations of complex ($(0.5–4.0) \times 10^{-5}$ mol dm^{-3}) at pH 4.0, μ = 0.1 mol dm^{-3}, and [bpy/phen/terpy] at 1.0×10^{-3} mol dm^{-3}.

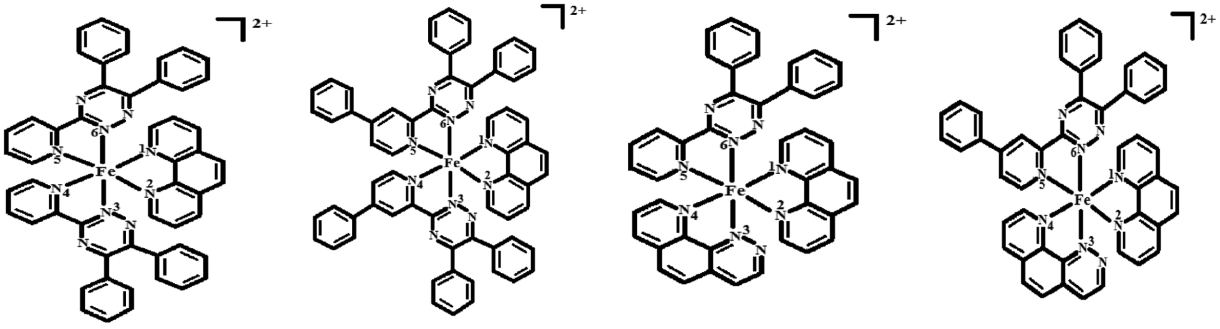

1 ($Fe(PDT)_2(phen)^{2+}$) **2** ($Fe(PPDT)_2(phen)^{2+}$) **3** ($Fe(PDT)(phen)_2^{2+}$) **4** ($Fe(PPDT)(phen)_2^{2+}$)

Scheme 2 Structural formulae of iron(II)-PDT/PPDT-phen mixed ligand complexes.

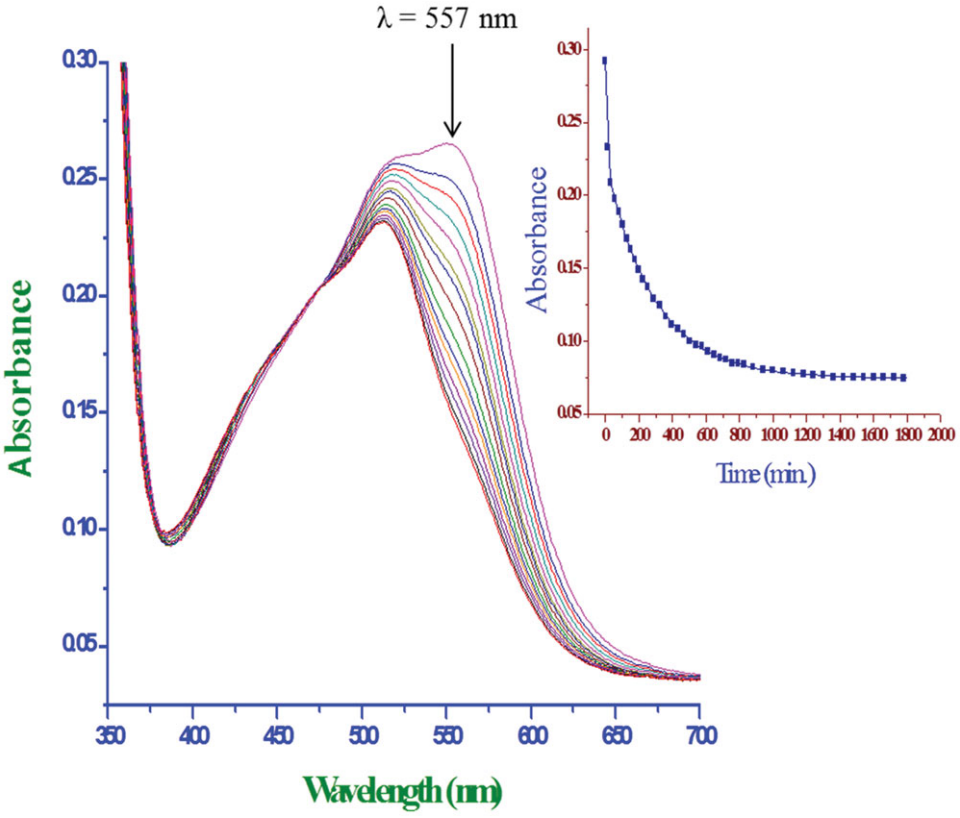

Figure 1 UV–vis spectral changes observed during the reaction between $Fe(PDT)_2(phen)^{2+}$ and phen: Inset is a typical kinetic trace at 557 nm. $[Fe(PDT)_2(phen)^{2+}] = 2.0 \times 10^{-5}$ mol dm^{-3}, [bpy] $= 1.0 \times 10^{-3}$ mol dm^{-3}, pH 4.0, $\mu = 0.2$ mol dm^{-3}, and temperature = 35°C. [Color figure can be viewed at wileyonlinelibrary.com]

The reactions were also carried out at various concentrations of bpy/phen/terpy ranging from 0.5×10^{-3} to 3.0×10^{-3} mol dm^{-3} and different pH values (3.6–5.6). The kinetic runs were performed at 25, 35, and 45°C to study the effect of temperature on the rate of these reactions. The spectral changes were monitored at 557 nm ($\varepsilon_{max} = 19{,}400 \pm 80$ mol^{-1} cm^{-1} dm^3), 567 nm ($\varepsilon_{max} = 22{,}800 \pm 100$ mol^{-1} cm^{-1} dm^3), 552 nm ($\varepsilon_{max} = 15{,}230 \pm 60$ mol^{-1} cm^{-1} dm^3), and 512 nm ($\varepsilon_{max} = 19{,}350 \pm 50$ mol^{-1} cm^{-1} dm^3), respectively, for complex **1**, **2**, **3**, and **4**. Figure 1 shows spectral changes for the substitution of $Fe(PDT)_2(phen)^{2+}$ by phen at 557 nm. Absorbance–time data at selected wavelengths were fitted to a single exponential

function, using the using Origin 7.5® graphical analysis software [30].

$$A_t = A_\infty + (A_0 - A_\infty)\exp^{(-k_{obs}t)} \quad (1)$$

where A_0, A_t, and A_∞ represent the absorbance of the reaction mixture initially, at time *t,* and at the end of the reaction, respectively.

The pseudo–first-order rate constant (k_{obs}) values from the single exponential fitting of data were reproducible to within ± 8%. A summary of the observed pseudo–first-order rate constant, k_{obs}, at different concentrations of complex and bpy/phen/terpy, pH, and ionic strength (μ) at 25, 35, and 45°C are presented in supplementary data S2, S3 and S4, respectively, in the Supporting Information.

Computational Modeling

Computational modeling was performed by the Gaussian 09 program package [31] to understand the structural and electronic differences and chemical transformations of the investigated complexes [32]. The geometry optimizations, frequency calculations, and molecular orbital generations were carried out by means of DFT using the B3LYP functional method [33,34]. The basis set 6–311+G* for nitrogen, 6–31G* for carbon and hydrogen [35], and Stuttgart-Dresden (SDD) basis for iron [36,37] was employed to get reliable results. The singlet state was used due to the low electronic spin of iron(II) complexes. The complexes were computed in water solution taking into account solvolysis effects by means of the conductor polarizable continue model [38,39]. All the structures were characterized as cationic species of formal charge 2+.

Species Distribution of the Substituting Ligands (bpy/phen/terpy)

Bpy and phen are monobasic and exist as mono- and unprotonated forms, whereas terpy is dibasic and exists as mono-, di-, and unprotonated forms in acidic media according to the following equilibria, respectively:

$$bpyH^+ \overset{k_a}{\rightleftharpoons} bpy + H^+ \quad (2)$$

$$phenH^+ \overset{k_a}{\rightleftharpoons} phen + H^+ \quad (3)$$

$$terpyH_2^+ \overset{k_{a_1}}{\rightleftharpoons} terpyH^+ + H^+ \quad (4)$$

$$terpyH_2^+ \overset{k_{a_2}}{\rightleftharpoons} terpyH^+ + H^+ \quad (5)$$

Bpy and phen have pK_a values of 4.54 [40] and 5.02 [41], respectively, at 25°C. Terpy is dibasic and has pK_{a_1} and pK_{a_2} values of 3.57 and 4.71 [42] at 25°C, respectively. Using these values, the percentage distribution of mono- and unprotonated forms of bpy and phen, mono-, and unprotonated and diprotonated forms of terpy were computed in the pH range from 3.6 to 5.6 using a simulation program [43]. The percentage distribution of bpy, phen, and terpy at the effective pH at which the substitution reactions was studied, the data are given in supplementary data S5 in the Supporting Information, whereas the species distribution curves are presented in supplementary data S6 in the Supporting Information. From the ligand distribution data S5 in the Supporting Information, it is clear that bpy, phen, and terpy exist mostly as monoprotonated species especially at the lower end of the pH 3.6–5.6 range. However, the unprotonated form of these ligands is considered as the reactive species.

Product Analysis

To characterize the products for the substitution of **1** to **4** by bpy, phen, and terpy, visible absorption spectra of solutions were recorded at the end of reactions. Requisite volumes of complex, bpy/phen/terpy, acetic acid–sodium acetate buffer, and sodium nitrate solutions were transferred into amber-colored 10 mL volumetric flasks and diluted to the mark with water. These solutions were left to stand for sufficient time to allow the reaction to complete. The visible absorbance spectra of complexes **1–4** and the reaction products with phen and terpy are shown in Figs. 2a and 2b.

Substitution products from the reactions of **1–4** with phen and terpy had absorption peaks at 510 nm (ε_{max} = 11,050 ± 100 mol^{-1} cm^{-1} dm^3) and 552 nm (ε_{max} = 12,400 ± 100 mol^{-1}cm^{-1} dm^3). The data suggest that complexes **1–4** react with phen and terpy to give $Fe(phen)_3^{2+}$ and $Fe(terpy)_2^{2+}$ as the final products, respectively (Fig. 2a), i.e., phen replaces the triazine ligand whereas terpy replaces both triazine and phen ligands from the iron(II) center. The molar absorptivities of the products at 510 and 552 nm were calculated on the basis of the concentration of iron(II) corresponding to that of $Fe(phen)_3^{2+}$ and $Fe(terpy)_2^{2+}$complexes, respectively.

The reaction products of bpy with complexes **1–4** gave results which were not similar to that observed for phen or terpy. If the triazine and phen ligands, which are coordinated on the iron(II) of the complexes, were all substituted by bpy to give $Fe(bpy)_3^{2+}$, a peak at λ_{max} = 522 nm (ε_{max} = 8,750 ± 50 mol^{-1} cm^{-1} dm^3)

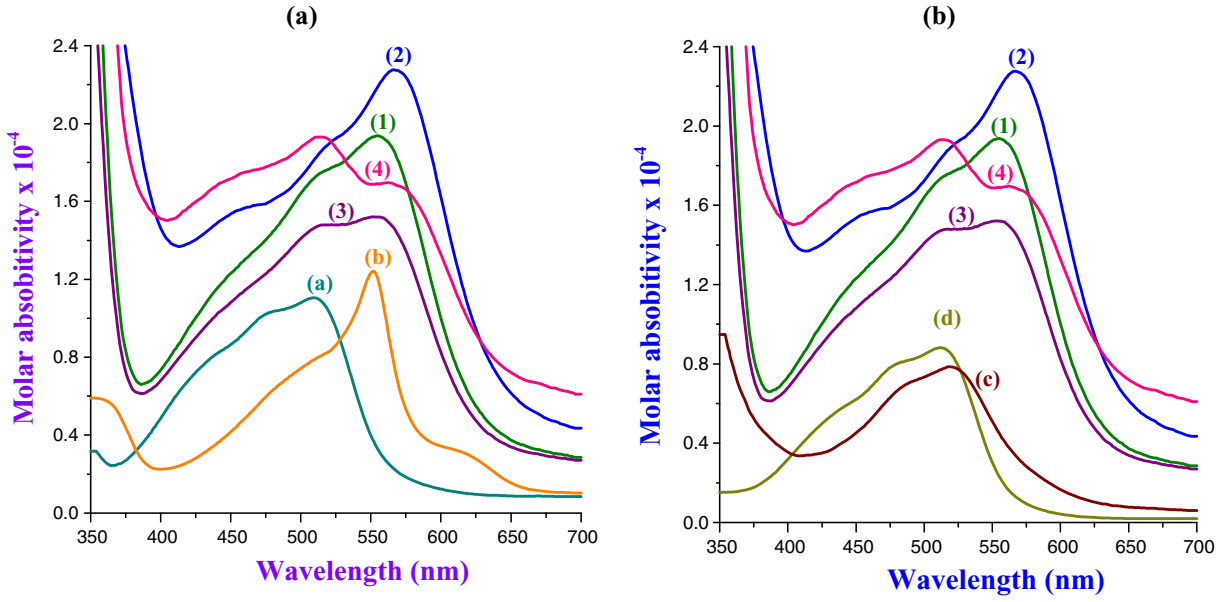

Figure 2 Visible absorption spectra of the reaction products of complexes **1**–**4** with phen/terpy (2a) and bpy (2b). where (1) = $Fe(PDT)_2(phen)^{2+}$, (2) = $Fe(PPDT)_2(phen)^{2+}$, (3) = $Fe(PDT)(phen)_2^{2+}$, (4) = $Fe(PPDT)(phen)_2^{2+}$, (a) = $Fe(phen)_3^{2+}$, (b) = $Fe(terpy)_2^{2+}$, (c) = $Fe(bpy)_2(phen)^{2+}$, and (d) = $Fe(bpy)(phen)_2^{2+}$. [Color figure can be viewed at wileyonlinelibrary.com]

would be expected. However, the substitution product of the reaction of complexes **1** or **2** with bpy showed a common absorption maximum at 517 nm (ε_{max} = 7,850 ± 150 mol^{-1} cm^{-1} dm^3) whereas that of complexes **3** or **4** with bpy showed a maximum at 513 nm (ε_{max} = 8,800 ± 120 mol^{-1} cm^{-1} dm^3). Based on this, it is clear that the substitution product was not the $Fe(bpy)_3^{2+}$ expected . It was postulated that only the triazines but not phen ligands were substituted from the complexes by bpy, resulting in the formation of iron(II) complexes containing phen and bpy. To ascertain this, the hypothesized products, $Fe(bpy)_2(phen)^{2+}$ and $Fe(phen)_2(bpy)^{2+}$, were synthesized and characterized by time-of-flight mass spectrometry (TOF-MS) and elemental analysis (mass spectra and other details are given in supplementary data S7 and S8, respectively, in the Supporting Information). The visible absorption spectra of pure solutions of $Fe(bpy)_2(phen)^{2+}$ and $Fe(phen)_2(bpy)^{2+}$ showed a λ_{max} at 517 nm (ε_{max} = 7,900 mol^{-1} cm^{-1} dm^3) and 513 nm (ε_{max} = 8,850 mol^{-1} cm^{-1} dm^3), respectively. The λ_{max} and ε_{max} values of the reaction products of complexes **1** or **2** with bpy agreed well with those of the synthesized $Fe(bpy)_2(phen)^{2+}$. Similarly, the λ_{max} and ε_{max} values for the products from the substitution of complexes **3** or **4** by bpy corresponded to those of $Fe(phen)_2(bpy)^{2+}$ within the experimental error (Fig. 2b).

The formation of mixed ligand complexes of the type $Fe(L_n)(L'_{3-n})^{x-}$ (where L = sulfonated phenyl-substituted triazines, L′ = phen, bpy, or terpy) [44] were reported in the study of substitution kinetics of iron(II)-sulfonated phenyl-substituted triazine complexes namely, $Fe(PDTS)_3^{4-}$ and $Fe(PPDTS)_3^{7-}$ by phen, bpy, and terpy. The intermediate complexes, $Fe(L_n)(L'_{3-n})^{x-}$ (where L = PDTS/PPDTS, L′ = phen, bpy, or terpy), were isolated using Dowex 50W-X8 cation-exchange and Dowex 1×8 anion-exchange resin columns. Earlier it had been found that the substitution of bis(2,4,6-tripyridyl 1,3,5- triazine)iron(II), $Fe(TPTZ)_2^{2+}$, by terpy [45] took place in two steps. The first step involves replacement of a TPTZ molecule by terpy forming an intermediate, $Fe(TPTZ)(terpy)^{2+}$, which further reacts with excess terpy to give the final product $Fe(terpy)_2^{2+}$. These authors prepared mixed ligand complex separately and followed the substitution kinetics with terpy. The specific rate constants, E_a and $\Delta S^{\#}$ values for the second step of reaction between $Fe(TPTZ)_2^{2+}$ with terpy and mixed ligand complex, $Fe(TPTZ)(terpy)^{2+}$ with terpy, are the same with in the experimental errors giving support to the envisaged mechanism. The literature vide supra and the present UV–vis data (λ_{max} and ε_{max} values), mass spectra, and elemental data confirm the formation of such mixed ligand complexes, namely $Fe(bpy)_2(phen)^{2+}$ (for **1** or **2**) or $Fe(phen)_2(bpy)^{2+}$ (for **3** or **4**) (Fig. 2b).

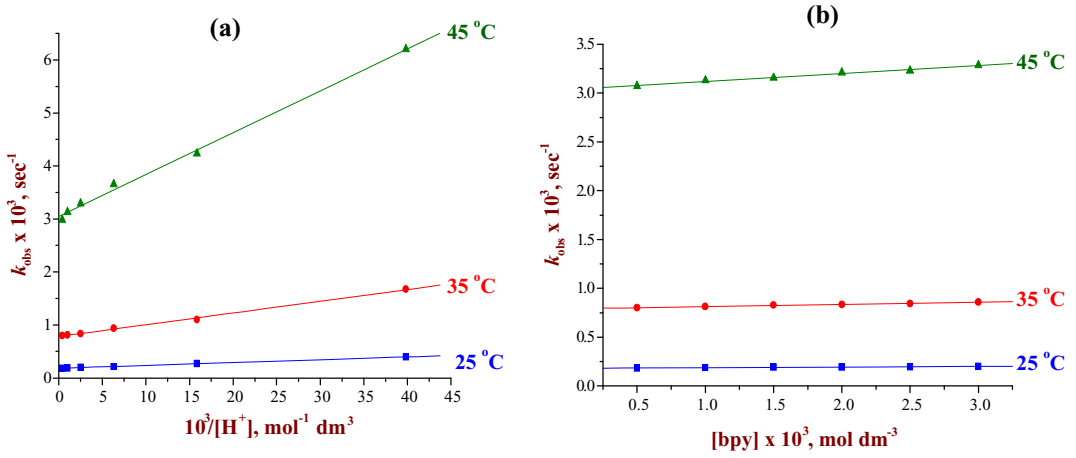

Figure 3 Linear plots of k_{obs} versus $1/[H^+]$ (a) and [bpy] (b) for the substitution of $[Fe(PDT)_2(phen)^{2+}]$ by bpy. $[Fe(PDT)_2(phen)^{2+}] = 2.0 \times 10^{-5}$ mol dm^{-3}, [bpy] $= 1.0 \times 10^{-3}$ mol dm^{-3}, pH 4.0, and $\mu = 0.2$ mol dm^{-3}. [Color figure can be viewed at wileyonlinelibrary.com]

RESULTS AND DISCUSSION

These reactions were carried out at 25, 35, and 45°C under pseudo–first-order conditions with [bpy/phen/terpy] ≫ [complex] in the pH range 3.6–5.6 in acetate buffers. The effect of concentration of complex, pH, bpy/phen/terpy, and ionic strength on these substitution was studied. Changing ionic strength evolved no effect on the reaction rate, but was dependent on [bpy/phen/terpy] and pH. Linear plots with positive slopes and large *y*-intercepts for k_{obs} versus [bpy/phen/terpy] and k_{obs} versus $1/[H^+]$ were observed. This suggests that these reactions proceed via two distinct paths (namely associative and dissociative) as well as being pH dependent. The representative plots of k_{obs} versus $1/[H^+]$ and k_{obs} versus [bpy] for the substitution of complex **1** by bpy are given in Figs. 3a and 3b, respectively. The linear plots of k_{obs} versus $1/[H^+]$ and k_{obs} versus [bpy/phen/terpy] for all other reactions are given in supplementary data S9 in the Supporting Information.

Proposed Mechanism for the Reaction of 1–4 and bpy/phen/terpy

The reactions of **1–4** by the entering ligands are summarized in Scheme 3.

These reactions were found to be first order with respect to concentration of complex, with ionic strength having no effect on the rate. This indicates that the rate-limiting step involves the reaction between an ion and a neutral species or two neutral species. The k_{obs} values increased with increasing [bpy/phen/terpy] and decreased with an increase in $[H^+]$. These observations support the mechanisms, which is outlined below.

Mechanism for the Reaction of 1 or 2 and bpy

Dissociative Path. Octahedral complexes generally undergo reversible dissociation. Thus, for the studied reactions, the formation of the pentavalent intermediate, defined by the rate constant, k_1, to give the intermediate, Fe(PDT/PPDT)(phen)(PDT/PPDT-η^1), is the rate-limiting step, and hence the rate of substitution is independent of incoming ligand. Looking at the structures of **1–4**, the ligand that has more bulk substituents (PDT/PPDT) is likely to dissociate faster from the iron(II) center to form a five-coordinated intermediate ahead of phen. The rate of dissociation of PDT/PPDT is controlled by the first-order dissociative rate constant, k_1 (read as *y*-intercepts of plots exemplified by Fig. 3, vide supra) as written in Eq. (6).

$$\mathrm{Fe\,(PDT/PPDT)_2\,(phen)^{2+}} \underset{k_{-1}}{\overset{k_1}{\rightleftharpoons}} \mathrm{Fe\,(PDT/PPDT)\,(phen)\,\left(PDT/PPDT-\eta^1\right)^{2+}} \quad (6)$$

where PDT/PPDT-η^1 is monodentate PDT/PPDT and $k_1 \gg k_{-1}$.

If bpy is taken in as an example, this five-coordinate intermediate reacts further with bpy molecules in a series of fast steps (7–9) to give $Fe(phen)(bpy)_2^{2+}$ as the final product.

$$\mathrm{Fe(PDT/PPDT)(phen)(PDT/PPDT-\eta^1)^{2+} + bpy} \overset{\text{fast}}{\rightarrow} \mathrm{Fe(PDT/PPDT)(phen)(PDT/PPDT-\eta^1)\,(bpy-\eta^1)^{2+}} \quad (7)$$

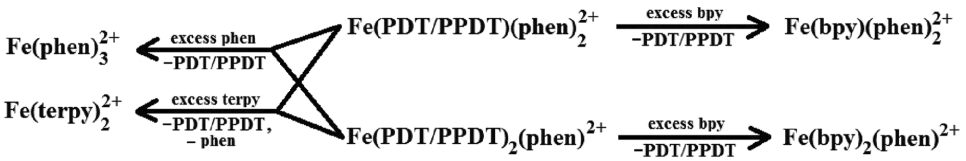

Scheme 3 The summarized substitution reactions with complexes **1–4** by bpy, phen, and terpy.

$$Fe(PDT/PPDT)(phen)(PDT/PPDT-\eta^1)(bpy-\eta^1)^{2+} \xrightarrow{fast} Fe(PDT/PPDT)(phen)(bpy)^{2+} + PDT/PPDT \quad (8)$$

Similarly, another molecule of PDT/PPDT dissociates from the product of Reaction (8) to give a series of intermediates, which are rapidly converted into the final product $Fe(phen)(bpy)_2^{2+}$ according to Eq. (9).

$$Fe(PDT/PPDT)(phen)(bpy)^{2+} + bpy \xrightarrow{fast} Fe(phen)(bpy)_2^{2+} + PDT/PPDT \quad (9)$$

Associative Path. In this mechanistic pathway, the incoming ligand (bpy) coordinates to the iron(II) center in the rate-determining step to form a seven-coordinated intermediate, $Fe(PDT/PPDT)_2(phen)(bpy\text{-}\eta^1)^{2+}$ as shown in Eq. (10),

$$Fe(PDT/PPDT)_2(phen)^{2+} + bpy \xrightarrow{slow,\ k_2} Fe(PDT/PPDT)_2(phen)(bpy-\eta^1)^{2+} \quad (10)$$

Subsequently, the seven coordinate intermediate rearranges itself wherein the bpy molecule chelates to iron(II) center whereas the PDT/PPDT dechelates to form $Fe(PDT/PPDT)(phen)(bpy)(PDT/PPDT\text{-}\eta^1)^{2+}$.

$$Fe(PDT/PPDT)_2(phen)(bpy-\eta^1) \xrightarrow{fast} Fe(PDT/PPDT)(phen)(bpy)(PDT/PPDT-\eta^1)^{2+} \quad (11)$$

This is followed by the decoordination of the monodentate PDT/PPDT from the iron(II).

$$Fe(PDT/PPDT)(phen)(bpy)(PDT/PPDT-\eta^1)^{2+} \xrightarrow{fast} Fe(PDT/PPDT)(phen)(bpy)^{2+} + PDT/PPDT \quad (12)$$

In a series of fast steps similar to (11) and (12), Fe(PDT/PPDT)(phen)(bpy) reacts with another molecule of bpy to give final product, $Fe(phen)(bpy)_2^{2+}$.

$$Fe(PDT/PPDT)(phen)(bpy)^{2+} + bpy \xrightarrow{fast} Fe(phen)(bpy)_2^{2+} + PDT/PPDT \quad (13)$$

Mechanism for the Reaction of 3 or 4 and bpy

The mechanisms for the substitution of $Fe(PDT/PPDT)(phen)_2$ by bpy are similar to that described for **1** or **2**. However, the complexes have only one replaceable ligand, i.e., PDT/PPDT; hence, the substitution paths for both the associative and dissociative steps terminate at Eqs. (8) and (12) respectively, to give $Fe(bpy)(phen)_2^{2+}$ as a final product.

$$Fe(PDT/PPDT)(phen)_2^{2+} + bpy \rightarrow Fe(bpy)(phen)_2^{2+} + PDT/PPDT \quad (14)$$

Further substitution of the mixed ligand complexes ($Fe(phen)(bpy)_2^{2+}$ and $Fe(bpy)(phen)_2^{2+}$) by another bpy molecule is not taking place in both dissociative and associative paths. This is probably because it is less basic than phen (see Table V and supplementary data S10 in the Supporting Information). Hence the reaction terminates via Eqs. (9) and (13) in associative and dissociative paths, respectively, to give a mixed ligand complex, $Fe(phen)(bpy)_2^{2+}$, as a final product.

Mechanism for the Reaction of 1–4 and phen or terpy

The mechanism for the substitution of **1–4** by phen is the same as described for bpy and proceeds to give $Fe(phen)_3^{2+}$ as a final product through Eqs. (9) and (13).

$$Fe(PDT/PPDT)_2(phen)^{2+} + 2phen \rightarrow Fe(phen)_3^{2+} + 2PDT/PPDT \quad (15)$$

$$\mathrm{Fe(PDT/PPDT)(phen)_2^{2+} + phen \rightarrow Fe(phen)_3^{2+} + PDT/PPDT} \quad (16)$$

The terpy ligand is less basic than bpy. However, it still substitutes both the triazines and phen ligands of **1–4** to form $Fe(terpy)_2^{2+}$ as the only final product.

$$\mathrm{Fe(PDT/PPDT)_2(phen)^{2+} + 2terpy \rightarrow Fe(terpy)_2^{2+} + 2PDT/PPDT + phen} \quad (17)$$

$$\mathrm{Fe(PDT/PPDT)(phen)_2^{2+} + 2terpy \rightarrow Fe(terpy)_2^{2+} + PDT/PPDT + 2phen} \quad (18)$$

Assuming that both paths take place, the rate law can be written as

$$\text{rate} = k_1\left[\text{complex}\right] + k_2\left[\text{complex}\right]\left[\text{bpy/phen/terpy}\right]_\text{e} \quad (19)$$

As already stated, under the present experimental conditions, bpy/phen/terpy ligands exist mostly in their monoprotonated form. Therefore,

$$\left[\text{bpy/phen/terpy}\right]_\text{t} = \left[\text{Hbpy}^+/\text{Hphen}^+/\text{Hterpy}^+\right]_\text{e} + \left[\text{bpy/phen/terpy}\right]_\text{e} \quad (20)$$

$[Hbpy^+/Hphen^+/Hterpy^+]_e$ and $[bpy/phen/terpy]_e$ are given from the ligand's (bpy/phen/terpy) protonation equilibria (Eqs. (2)–(4)),

$$[\text{Hbpy}^+/\text{Hphen}^+/\text{Hterpy}^+]_\text{e} = \frac{[\text{bpy/phen/terpy}]_e[\text{H}^+]_\text{e}}{K_a} \quad (21)$$

Substituting Eqs. (21) into (20),

$$[\text{bpy/phen/terpy}]_e = \frac{K_a[\text{bpy/phen/terpy}]_\text{t}}{K_a + [\text{H}^+]_\text{e}} \quad (22)$$

Thus, Eq. (19) becomes

$$\text{Rate} = k_1[\text{complex}] + \frac{k_2K_a[\text{complex}][\text{bpy/phen/terpy}]_\text{t}}{K_a + [\text{H}^+]_\text{e}} \quad (23)$$

$$= [\text{complex}]\left\{k_1 + \frac{k_2K_a[\text{bpy/phen/terpy}]_\text{t}}{K_a + [\text{H}^+]_\text{e}}\right\} \quad (24)$$

If the terms $[bpy/phen/terpy]_t$ and $[H^+]_e$ are replaced by [bpy/phen/terpy] and $[H^+]$ (initial concentrations of bpy/phen/terpy and H^+), respectively,

$$\text{Rate} = [\text{complex}]\left\{k_1 + \frac{k_2K_a[\text{bpy/phen/terpy}]}{K_a + [\text{H}^+]}\right\} \quad (25)$$

$$\text{Therefore, } k_\text{obs} = k_1 + \frac{k_2K_a[\text{bpy/phen/terpy}]}{K_a + [\text{H}^+]} \quad (26)$$

By neglecting the term K_a, since $[H^+] \gg K_a$ Eq. (27) becomes

$$k_\text{obs} = k_1 + \frac{k_2K_a[\text{bpy/phen/terpy}]}{[\text{H}^+]} \quad (27)$$

This equation satisfies all the experimental observations, such as plots of k_{obs} versus $1/[H^+]$ or [bpy/phen/terpy], which are straight lines with positive slopes and intercepts, as shown in Figs. 3a and 3b. The y-intercept of both plots gives the first-order dissociative rate constants, k_1. The second-order rate constants, k_2, for the associative path are calculated from either the slope of the plots of k_{obs} versus $1/[H^+]$ (slope $= k_2K_a$[bpy/phen/terpy]) or k_{obs} vs. [bpy/phen/terpy] (slope $= k_2K_a/[H^+]$). Protonation constant, K_a, values for bpy, phen, and terpy at 25°C are obtained from the literature [40–42], whereas at higher temperatures (at 35 and 45°C) the Perrin equation [46] shown in Eq. (28) was used to evaluate their values,

$$\frac{\Delta \text{p}K_\text{a}}{\Delta T} = \frac{\text{p}K_\text{a} - 0.9}{T} \quad (28)$$

where T is in kelvins. Using the specific rate constants (k_1 and k_2), the activation parameters (E_a, $\Delta H^\#$, $\Delta S^\#$, and $\Delta G^\#$) for both paths were computed using Arrhenius and Eyring equations [47] at the three temperatures. Specific rate constant and activation parameter values for both dissociative and associative paths are given in Tables II and III, respectively. Irrespective of ligands (see Table II), the calculated specific rate constants (k_1) are constant and independent of concentration of the ligand, i.e. the dissociative path of the complex is not effected by the nature of the incoming ligand. The energy of activation (E_a) or enthalpy ($\Delta H^\#$) decreases from complex **1–4** in line with the decrease in steric bulk or number of coordinated PDT/ PPDT in complexes **1–4**. As a consequent, k_1 values marginally increase in the order **1** < **2** < **3** < **4**. The dissociative path was confirmed by $+\Delta S^\#$ values (Table II); these values also decrease from **1** to **4**, again confirming

Table II Specific Rate Constants and Activation Parameters for Dissociative Path of the Reaction

	Dissociative path, $k_1 \times 10^3$ (s^{-1})											
	Bpy				phen				terpy			
Parameter	**1**	**2**	**3**	**4**	**1**	**2**	**3**	**4**	**1**	**2**	**3**	**4**
Temperature (°C)												
25	0.18 ± 0.03	0.22 ± 0.04	0.34 ± 0.03	0.39 ± 0.07	0.19 ± 0.01	0.22 ± 0.03	0.33 ± 0.01	0.39 ± 0.02	0.18 ± 0.02	0.22 ± 0.05	0.32 ± 0.01	0.38 ± 0.03
35	0.79 ± 0.07	0.92 ± 0.05	1.30 ± 0.09	1.44 ± 0.08	0.78 ± 0.06	0.91 ± 0.04	1.32 ± 0.07	1.45 ± 0.08	0.79 ± 0.05	0.91 ± 0.06	1.31 ± 0.08	1.43 ± 0.07
45	3.06 ± 0.11	3.41 ± 0.15	4.60 ± 0.09	5.10 ± 0.17	3.04 ± 0.09	3.39 ± 0.13	4.61 ± 0.11	5.19 ± 0.10	3.05 ± 0.14	3.40 ± 0.09	4.61 ± 0.10	5.04 ± 0.13
E_a (kJ mol^{-1})	115 ± 3	108 ± 2	103 ± 2	101 ± 3	113 ± 2	106 ± 2	101 ± 3	99 ± 1	115 ± 5	103 ± 2	100 ± 3	99 ± 1
$\Delta H^{\#}$ (kJ mol^{-1})	119 ± 2	106 ± 4	101 ± 3	99 ± 3	118 ± 1	104 ± 4	100 ± 1	97 ± 3	117 ± 1	105 ± 2	101 ± 1	97 ± 3
$\Delta S^{\#}$ (J K^{-1} mol^{-1})	48 ± 13	40 ± 8	27 ± 5	22 ± 9	46 ± 13	39 ± 7	28 ± 10	20 ± 9	45 ± 7	41 ± 10	26 ± 6	21 ± 8
$\Delta G^{\#}_{35°C}$ (kJ mol^{-1})	94 ± 3	94 ± 1	93 ± 2	93 ± 2	94 ± 1	93 ± 1	94 ± 2	94 ± 1	93 ± 2	93 ± 3	94 ± 1	93 ± 2

Table III Specific Rate Constants and Activation Parameters for Associative Path of the Reaction

	Associative path, $k_2 \times 10^1$ (mol dm^{-3} s^{-1})											
	bpy				phen				terpy			
Parameter	**1**	**2**	**3**	**4**	**1**	**2**	**3**	**4**	**1**	**2**	**3**	**4**
Temperature (°C)												
25	0.22 ± 0.02	0.37 ± 0.01	0.66 ± 0.03	1.11 ± 0.02	0.98 ± 0.01	1.73 ± 0.03	3.52 ± 0.04	6.17 ± 0.03	0.40 ± 0.03	0.70 ± 0.03	1.36 ± 0.02	2.28 ± 0.01
35	0.59 ± 0.05	0.89 ± 0.03	1.53 ± 0.07	2.30 ± 0.06	2.52 ± 0.05	4.03 ± 0.08	7.28 ± 0.08	11.80 ± 0.06	1.01 ± 0.09	1.60 ± 0.05	2.84 ± 0.03	4.58 ± 0.06
45	1.48 ± 0.09	2.00 ± 0.12	2.94 ± 0.17	4.59 ± 0.08	5.88 ± 0.20	8.15 ± 0.16	12.6 ± 0.14	21.03 ± 0.09	2.00 ± 0.11	3.58 ± 0.14	5.49 ± 0.22	8.81 ± 0.17
E_a (kJ mol^{-1})	75 ± 3	66 ± 2	59 ± 2	56 ± 1	71 ± 2	61 ± 1	50 ± 3	48 ± 1	74 ± 4	64 ± 1	55 ± 2	54 ± 3
$\Delta H^{\#}$ (kJ mol^{-1})	73 ± 4	64 ± 1	56 ± 2	53 ± 3	68 ± 1	59 ± 3	48 ± 2	46 ± 2	71 ± 3	62 ± 2	52 ± 2	51 ± 1
$\Delta S^{\#}$ (J K^{-1} mol^{-1})	–33 ± 8	–59 ± 11	–78 ± 9	–85 ± 13	–36 ± 9	–63 ± 8	–93 ± 10	–95 ± 8	–34 ± 8	–61 ± 9	–86 ± 13	–87 ± 9
$\Delta G^{\#}_{35°C}$ (kJ mol^{-1})	83 ± 1	82 ± 1	81 ± 2	79 ± 1	79 ± 1	78 ± 2	77 ± 1	75 ± 1	81 ± 1	80 ± 2	79 ± 2	78 ± 1

Table IV Log k_2 Values for the Reactions of the Complexes **1–4** and the pK_a Values of the bpy, phen, and terpy at 35°C

		2+log k_2			
Ligand	pK_a	**1**	**2**	**3**	**4**
bpy	4.42	0.77	0.95	1.19	1.36
phen	4.89	1.40	1.61	1.86	2.07
terpy	4.59	1.01	1.20	1.45	1.66

the above order of reactivity of the complexes. The $\Delta G^{\#}_{35°C}$ values of complexes **1–4** suggest that all these reactions essentially follow the same mechanism.

The rate constants, k_2, (Table III) depend on the concentration of the entering ligand (vide supra), indicating that their activated states are bimolecular. The k_2 values for the associative path increase from complexes **1** to **4** (Table IV) for the substitution of labile ligands, and hence the order of reactivity is **1** < **2** < **3** < **4**. The $\Delta H^{\#}$ decreases from complex **1** to **4**, supporting the above reactivity order. The negative $\Delta S^{\#}$ values are also observed. The order of reactivity with respect to incoming ligands is phen > terpy > bpy. The reactivity of the incoming ligands correlates well with their basicity. The pK_a of the N-donor heterocyclic nucleophiles at 25°C decreases in the order: phen [41] (5.02) > terpy [42] (4.71) > bpy [40] (4.54).

Since phen is the most basic of the three ligands (see Table IV and supplementary data S10 in the Supporting Information), neither bpy nor terpy is expected to replace the phen molecules from complexes **1–4**. As expected, the spectral data of the products from reactions of complexes **1–4** with bpy (see Fig. 2b) confirm the replacement of only the triazines but not the phen to form the mixed ligand complexes $(Fe(bpy)_2(phen)^{2+}$ and $Fe(phen)_2(bpy)^{2+})$ as final products. These were also confirmed independently. Despite terpy being less basic than phen, it replaced both the triazine and phen from iron(II) center as confirmed by spectral data. This anomaly is attributed to (with respect to the observed order of reactivity) to terpy's tridentate-chelating ability leading to the ultimate formation of the thermodynamically favoured$Fe(terpy)_2^{2+}$as the final product.

The pK_a and log k_2 at 35°C are presented in Table V and the data for other temperatures (25 and 45°C) are given in supplementary data S10 in the Supporting Information. When the pK_a data of the ligands were plotted against log k_2, according to Eq. (29) [48], straight line plots were obtained as shown in Fig. 4 and supplementary data S11 in the Supporting Information.

$$\log k_2 = \alpha\,(pK_a) + b \qquad (29)$$

where α and b are the electronic and steric effects.

The straight line plots of log k_2 versus pK_a of incoming ligands (see Fig. 4 and supplementary data S11 in the Supporting Information) confirm a linear free energy relationship (LFER) between basicity and the reactivity of nucleophiles [48].

The slope of the plots (Fig. 4) is a measure of the electrophilicity of the metal center, which in turn describes the ability of the Fe(II) center to discriminate between incoming ligands [49,50]. The slopes of the plots at 35°C increase in the following order: **1** (1.336) < **2** (1.388) < **3** (1.433) < **4** (1.498), indicating the order of ability of the complexes to discriminate among the incoming ligands.

Generally, the substitution reactions at the iron(II) center occur by both dissociative and associative paths [51,52]. Between these two paths, the former is more preferred for the iron(II)–polypyridyl complexes through the formation of aqua intermediate in the rate-determining step, which gives the final product in a series of fast steps [53,54]. Such a behavior was reported for the substitution of $Fe(bpy)_2(CN)_2$ by phen in which the formation of intermediate, $Fe(bpy)(CN)_2(H_2O)_2$, was postulated [55]. In the present study, there is no evidence for the formation of such an aqua intermediate complex. If there was a chance to form such an intermediate, the rate of substitution would be very fast, but the reaction rates are of the order of 10^{-3} s^{-1} at 35°C. It clearly indicates that the low-spin character of the complex is not disturbed at any stage of reaction, and hence it can be concluded that these reactions essentially occur by an associative mechanism. Smaller k_1, large $\Delta H^{\#}$ values are noticed for the dissociative path than the associative path. Smaller $\Delta H^{\#}$ values means that the reaction is easier on energy grounds. Positive $\Delta S^{\#}$ values are obtained for the dissociative path, whereas negative values were noted for the associative path. Large negative entropy values indicate the formation of a highly ordered and more compact seven-coordinate activated complex in the reaction path [44,56]. The k_2, $\Delta H^{\#}$or E_a and $-\Delta S^{\#}$ values support the associative character of these reactions.

Computational Analysis

Computational DFT calculations were performed to get in-depth understanding of the structural as well electronic differences of the complexes. The descriptors such as ionization potential (I), electron affinity (A), chemical hardness (η), chemical softness (σ), chemical potential (μ), and dipole moment to help explain the observed reactivity trend of the complexes investigated in the present study. The DFT calculated geometry-optimized structures and frontier orbital

Table V DFT-Calculated Data for Investigated Complexes

Complex	1	2	3	4
MO energy (eV)				
$I = -E_{HOMO}$	6.574	6.535	6.468	6.455
$A = -E_{LUMO}$	3.236	3.218	3.179	3.178
$\Delta E_{LUMO\text{-}HOMO}$	3.339	3.317	3.289	3.277
NBO charge				
Fe^{2+}	0.250	0.249	0.271	0.271
N_{phen}	−0.407	−0.406	−0.424	−0.423
N_{phen}	−0.407	−0.405	−0.406	−0.405
N	−0.205	−0.205	−0.425	−0.424
N	−0.421	−0.425	−0.421	−0.421
$N_{pyridyl}$	−0.421	−0.425	−0.422	−0.426
$N_{triazine}$	−0.204	−0.203	−0.201	−0.201
Bond lengths				
Fe-N_{phen}	2.008	2.008	2.013	2.012
Fe-N_{phen}	2.008	2.004	2.007	2.007
Fe-N	1.957	1.958	2.015	2.015
Fe-N	2.010	2.007	2.012	2.014
Fe-$N_{pyridyl}$	2.010	2.007	2.010	2.007
Fe-$N_{triazine}$	1.957	1.957	1.953	1.952
Chemical hardness (η)	1.669	1.658	1.645	1.639
Chemical softness (σ)	0.599	0.603	0.608	0.610
Electronegativity ($\chi = -\mu$)	4.905	4.876	4.824	4.817
Dipole moment (D)	2.873	3.589	10.534	10.698

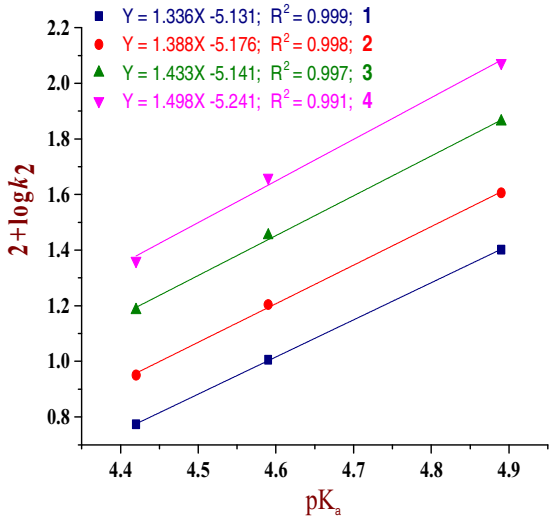

Figure 4 Plot of log k_2 obtained for the substitution reactions against the pK_a values of the bpy, phen, and terpy at 35°C. [Color figure can be viewed at wileyonlinelibrary.com]

energy (highest occupied molecular orbital, HOMO and lowest molecular orbital, LUMO) maps along with data are summarized in Fig. 5 and Table V, respectively. The DFT-calculated frontier orbital diagrams show that most of the HOMO electron density is from d-orbitals of iron atom and partially from conjugated π-system of the pyridyl rings in PDT/PPDT molecule. The LUMO electron density is primarily from the π-electron system of the ligand and a smaller contribution from the d-orbitals on Fe center. It is observed that the HOMOs and LUMOs of all complexes, the π-electron system of the ligands (PDT/PPDT), and d-orbitals of iron have major contribution to the substitution process, whereas the phen molecules are quite inert which indicates that these substitution reactions are significantly depend on PDT/PPDT ligands.

From the above table, the bond lengths of Fe-N_{phen} is in the same order for all the four complexes, indicating that the flow of electrons from phen to metal is uniform and phen molecule has no effect on the reactivity of the complexes. A similar conclusion was also drawn from the HOMO and LUMO maps of the complexes. Since the associative path predominates ($k_2 \approx 100k_1$ for all reactions) the DFT calculations will be discussed in support of an associative mechanism only.

The difference in the reactivity of the complexes is mainly due to the difference in the number of phenyl groups on the triazine ring. From Table V, Fe-$N_{triazine}$ bond length (~1.95) was significantly less compared to the Fe-$N_{pyridyl}$ (~2.01) and Fe-N_{phen} (~2.01). This

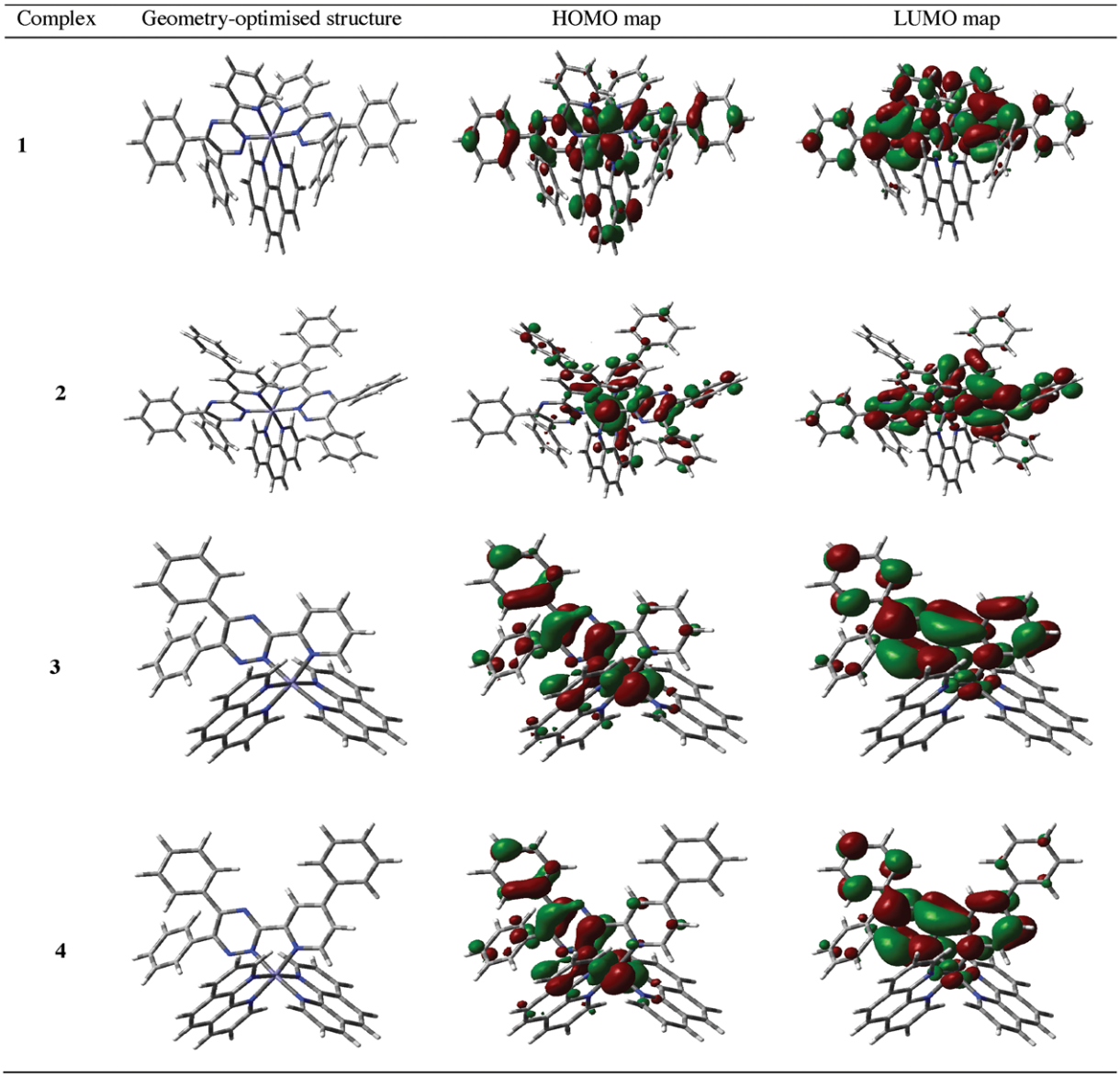

Figure 5 DFT-optimized frontier orbital energy structures, HOMO and LUMO maps for iron(II) complexes at the B3LYP/SDD level. [Color figure can be viewed at wileyonlinelibrary.com]

is due to a flow of electrons from the ligand leading to a shorter and strong bond. Natural bond orbital, NBO charge is a measure of π-electron delocalization and shows the degree of the aromaticity of the atom aromatic rings [57,58]. The flow of electrons from phenyl rings of $N_{triazine}$ to metal causing increased electron density on the metal center, resulting in less positive NBO charges on Fe^{2+}. Because of the nonuniform flow of electrons via $N_{triazine}$ and $N_{pyridyl}$ of the PDT/PPDT bidentate ligands, one end of the ligand can decoordinate from the Fe^{2+} center to form a monodentate PDT/PPDT at the Fe(II) center. Under pseudo–first-order conditions ([incoming ligand] $\gg$ [complex]), the formation of new bond with incoming ligand and dissociation of triazine molecule (PDT/PPDT) from the Fe^{2+} center occurs simultaneously to form an intermediate which undergo further reactions to give the final product in a series of fast steps.

The electronic effects of the inert ligand on the rate of substitution at square planar platinum complexes including their reactivity have been explained using NBO charge on the metal center [59–62]. For associative substitution, the complexes with high positive NBO charges on the metal center are highly reactive

toward incoming ligands. In the present study, complexes **1** and **2** have similar NBO charges on Fe^{2+} (0.250), which are significantly less than those of complexes **3** and **4** (0.270). The lower NBO charge for complexes **1** and **2** is due to the presence of more poor π-acceptors of electron density (two PDT/PPDT molecules and one phen) around the metal center compared to **3** and **4** (one PDT/PPDT and two phen). Phenyl groups on the triazines of PDT/PPDT release electrons to the nitrogen thereby deactivating the iron(II) toward nucleophilic substitution [63]. Thus, complexes with more number of PDT/PPDT have less NBO charges on the metal center and are less reactivity toward the incoming molecule. This corroborates the experimentally observed trend.

The energy of HOMO and LUMO are associated with the electron-donating and electron-accepting abilities of the complexes, respectively [64,65]. The complexes with smaller HOMO–LUMO energy gap are reactive and kinetically labile [66,67]. This is also the case in the present study, where the HOMO–LUMO energy gap gradually decreases from complex **1** to **4** as the reactivity increases. Electron descriptors [68,69] such as ionization potential (I), electron affinity (A), electronegativity $(\chi) = (I + A)/2$, hardness $(\eta) = (I - A)/2$ and softness $(\sigma) = 1/\eta$, and dipole moment were calculated from the DFT data. Higher ionization potential or negative chemical potential energy, high chemical hardness (large HOMO–LUMO gap), and low softness (small HOMO–LUMO gap) values are observed for complex **1** compared to the rest. This complex is relatively more stable and kinetically inert than the rest. The electron descriptors data for complexes **1–4** corroborates well with the order of reactivity: **1** < **2** < **3** < **4**. The reactivity of the complexes (**1–4**) also had a direct relationship with dipole moment. The dipole moment increased with an increase in polarizability or a decrease in the HOMO–LUMO energy gap of the complexes [70–72]. Complex **1** has the lowest dipole moment (2.873) and **4** has the highest dipole moment (10.698) in line with the trend in the reactivity.

CONCLUSIONS

The substitution of bpy/phen/terpy occurs by both dissociative and associative mechanisms. However, the higher k_2, smaller $\Delta H^{\#}$, and large negative $\Delta S^{\#}$ values for associative path clearly indicates that these substitution reactions proceeded predominantly by the associative mechanism. The phenyl groups present in the triazine molecule(s) decrease the reactivity of the complexes due to inductive donation of electrons from the phenyl rings to the metal center via the coordinated nitrogen atom of the triazine ligands. This is seen in the decrease in NBO charge on Fe(II) as the number of phenyl groups of the triazine ligands coordinated to the metal center increases. DFT-calculated HOMO–LUMO gap, NBO charges on Fe^{2+}, and electron descriptors data support the reactivity order of the complexes: **1** < **2** < **3** < **4**. The rate constants (k_1 and k_2) increase from complexes **1** to **4** supporting the above order of reactivity. The LFER exists between the basicity of the incoming ligand and their order of reactivity with the complexes. The rate of substitution of the triazine ligand by the incoming ligands (phen/terpy/bpy) increases in the order phen > terpy > bpy.

The author Rajesh Bellam, postdoctoral fellow, is gratefully indebted to the University of KwaZulu-Natal, South Africa, for the financial support.

BIBLIOGRAPHY

1. Blau, F. Ber Dtsch Chem Ges 1888, 21, 1077–1078.
2. Blau, F. Monatsh Chem/Chem Mon 1898, 19, 647–689.
3. Moss, M. L.; Mellon, M. G. Ind Eng Chem Anal Ed 1942, 14, 862–865.
4. Case, F. H.; Koft, E. J Am Chem Soc 1959, 81, 905–906.
5. Neunhoeffer, H.; Wiley, P. F. The Chemistry of Heterocyclic Compounds, Chemistry of 1 2 3-Triazines and 124-Triazines, Tetrazines, and Pentazin; Wiley: Hoboken, NJ, 2009.
6. Arshad, M.; Khan, T. A.; Khan, M. A. ChemInform 2015, 46, 149–162.
7. Catozzi, N.; Edwards, M. G.; Raw, S. A.; Wasnaire, P.; Taylor, R. J. J Org Chem 2009, 74, 8343–8354.
8. Holla, B. S.; Gonsalves, R.; Rao, B. S.; Shenoy, S.; Gopalakrishna, H. Il farmaco 2001, 56, 899–903.
9. Makki, M. S. T.; Rahman, R. M. A.; Ali, O. A. A. Int J Org Chem 2015, 5, 153–165.
10. Hay, M. P.; Pruijn, F. B.; Gamage, S. A.; Liyanage, H. S.; Kovacs, M. S.; Patterson, A. V.; Wilson, W. R.; Brown, J. M.; Denny, W. A. J Med Chem 2004, 47, 475–488.
11. Lübbers, T.; Angehrn, P.; Gmünder, H.; Herzig, S.; Kulhanek, J Bioorg Med Chem Lett 2000, 10, 821–826.
12. Baliani, A.; Bueno, G. J.; Stewart, M. L.; Yardley, V.; Brun, R.; Barrett, M. P.; Gilbert, I. H. J Med Chem 2005, 48, 5570–5579.
13. El-Gendy, Z.; Morsy, J.; Allimony, H.; Ali, W.; Abdel-Rahman, R. Die Pharm 2001, 56, 376–383.
14. Mullick, P.; Khan, S. A.; Begum, T.; Verma, S.; Kaushik, D.; Alam, O. Acta Pol Pharm Drug Res 2009, 66, 379–385.
15. Abdel-Rahman, R. M.; Makki, M. S.; Ali, T. E.; Ibrahim, M. A. J Hetrocyclic Chem 2015, 52, 1595–1607.
16. Chriswell, C.; Schilt, A. Anal Chem 1974, 46, 992–996.
17. Schilt, A. A.; Hoyle, W. C. Anal Chem 1967, 39, 114–117.
18. Schilt, A. A. J Am Chem Soc 1960, 82, 3000–3005.

19. Taylor, P.; Schilt, A. Inorg Chim Acta 1971, 5, 691–697.
20. Burgess, J.; Haines, R. I. J Chem Soc, Dalton Trans 1978, 1447–1451.
21. Baker Jr, W.; Bobonich, H. Inorg Chem 1963, 2, 1071–1072.
22. Múñoz, E.; Graciani, M. D. M.; Jiménez, R.; Rodríguez, A.; Moyá, M. L.; Sánchez, F. Int J Chem Kinet 1994, 26, 299–307.
23. Blake, R.; White, K. J.; Shute, E. A. J Biol Chem 1991, 266, 19203–19211.
24. Balasubramanian, S. Syn React Inorg Met-Org Chem 1999, 29, 377–394.
25. Kobetić, R.; Denžić, M.; Zimmermann, B.; Rončević, S.; Baranović, G. J Coord Chem 2012, 65, 3433–3448.
26. Wijaya, K.; Yoshioka, N.; Inoue, H. J Inorg Biochem 2003, 94, 263–271.
27. Wijaya, K.; Wahyuni, E. T.; Yoshioka, N.; Inoue, H. Biophys Chem 2006, 121, 44–50.
28. Mudasir, M.; Wijaya, K.; Wahyuni, E. T.; Inoue, H. Ind J Chem 2010, 4, 174–179.
29. Stookey, L. L. Anal Chem 1970, 42, 779–781.
30. Origin7.5TM SRO, v7.5714 (B5714); Origin Lab Corporation: Northampton, OH, 2003.
31. Frisch, M.; Trucks, G.; Schlegel, H.; Scuseria, G.; Robb, M.; Cheeseman, J.; Scalmani, G.; Barone, V.; Mennucci, B.; Petersson, G. Gaussian Inc.: Wallingford CT, Gaussian Manual, 2009.
32. Reed, A. E.; Weinstock, R. B.; Weinhold, F. J Chem Phy 1985, 83, 735–746.
33. Becke, A. D. J Chem Phy 1993, 98, 5648–5652.
34. Lee, C.; Yang, W.; Parr, R. G. Phy Rev B 1988, 37, 785–789.
35. Hehre, W. J.; Ditchfield, R.; Pople, J. A. J Chem Phys 1972, 56, 2257–2261.
36. Fuentealba, P.; Preuss, H.; Stoll, H.; Von Szentpály, L. Chem Phy Lett 1982, 89, 418–422.
37. Sameera, W.; Hatanaka, M.; Kitanosono, T.; Kobayashi, S.; Morokuma, K. J Am Chem Soc 2015, 137, 11085–11094.
38. Chval, Z.; Sip, M.; Burda, J. V. J Comp Chem 2008, 29, 2370–2381.
39. Cossi, M.; Rega, N.; Scalmani, G.; Barone, V. J Comp Chem 2003, 24, 669–681.
40. Brandt, W. W.; Dwyer, F. P.; Gyarfas, E. D. Chem Rev 1954, 54, 959–1017.
41. Daniele, P. G.; Rigano, C.; Sammartano, S. Talanta 1985, 32, 78–80.
42. Brandt, W. W.; Wright, J. P. J Am Chem Soc 1954, 76, 3082–3083.
43. Alderighi, L.; Gans, P.; Ienco, A.; Peters, D.; Sabatini, A.; Vacca, A. Coord Chem Rev 1999, 184, 311–318.
44. Bellam, R.; Anipindi, N. R. Trans Met Chem 2014, 39, 311–326.
45. Rao, G. V.; Bellam, R.; Anipindi, N. R. Trans Met Chem 2012, 37, 189–196.
46. Perrin, D. Aust J Chem 1964, 17, 484–488.
47. Evans, M. G.; Polanyi, M. Trans Faraday Soc 1935, 31, 875–894.
48. Pitteri, B.; Bortoluzzi, M. Polyhedron 2006, 25, 2698–2704.
49. Bellicini, M.; Cattalini, L.; Marangoni, G.; Pitteri, B. J Chem Soc, Dalton Trans 1994, 1805–1811.
50. Pitteri, B.; Marangoni, G.; Cattalini, L.; Visentin, F.; Bertolasi, V.; Gilli, P. Polyhedron 2001, 20, 869–880.
51. Gardner, E. R.; Mekhail, F. M.; Burgess, J.; Rankin, J. M. J Chem Soc, Dalton Trans 1973, 1340–1344.
52. Burgess, J. J Chem Soc, Dalton Trans 1972, 1061–1063.
53. Broomhead, J.; Dwyer, F. J Chem 1961, 14, 250–252.
54. Basolo, F.; Dwyer, F. P. J Am Chem Soc 1954, 76, 1454–1455.
55. Burgess, J. J Chem Soc, Dalton Trans 1972, 203–206.
56. Visweswara Rao, G.; Sridhar, Y.; Hela, P. G.; Padhi, T.; Anipindi, N. R. Trans Met Chem 1999, 24, 566–570.
57. Matulis, V. E.; Halauko, Y. S.; Ivashkevich, O. A.; Gaponik, P. N. J Mol Struct: THEOCHEM 2009, 909, 19–24.
58. Kuznetsov, M.; Bokach, N.; Kharlampidi, D.; Medvedev, Y. N.; Kukushkin, V. Y.; Dementiev, A. Russ J Gen Chem 2010, 80, 458–467.
59. Shaira, A.; Jaganyi, D. J Coord Chem 2014, 67, 2843–2857.
60. Kinunda, G.; Jaganyi, D. Trans Met Chem 2014, 39, 939–949.
61. Wekesa, I. M.; Jaganyi, D. J Coord Chem 2016, 389–403.
62. Khusi, B. B.; Mambanda, A.; Jaganyi, D. Trans Met Chem 2016, 41, 191–203.
63. Bellam, R.; Raju, G. G.; Anipindi, N. R.; Jaganyi, D. Trans Met Chem 2016, 41, 271–278.
64. Musa, A. Y.; Kadhum, A. A. H.; Mohamad, A. B.; Rahoma, A. A. B.; Mesmari, H. J Mol Struct 2010, 969, 233–237.
65. Kuznetsov, M. L.; Kukushkin, V. Y.; Haukka, M.; Pombeiro, A. J. Inorg Chim Acta 2003, 356, 85–94.
66. Kuznetsov, M. L.; Bokach, N. A.; Kukushkin, V. Y.; Pakkanen, T.; Wagner, G.; Pombeiro, A. J. J Chem Soc, Dalton Trans 2000, 4683–4693.
67. Gece, G.; Bilgiç, S. Corros Sci 2009, 51, 1876–1878.
68. Parr, R. G.; Pearson, R. G. J Am Chem Soc 1983, 105, 7512–7516.
69. Pearson, R. G. Inorg Chem 1988, 27, 734–740.
70. Atkins, P.; De Paula, J. Physical Chemistry for the Life Sciences; Oxford University Press: New York, 2011.
71. Islam, M. M.; Bhuiyan, M. D. H.; Bredow, T.; Try, A. C. Comp Theor Chem 2011, 967, 165–170.
72. Parimala, K.; Balachandran, V. Spectrochimica Acta Part A 2011, 81, 711–723.